

Main sequence of star formation and colour bimodality considering galaxy environment

Pius Privatus^{1,2,*} and Umananda Dev Goswami^{1,†}

¹*Department of Physics, Dibrugarh University, Dibrugarh 786004, Assam, India*

²*Department of Natural Sciences, Mbeya University of Science and Technology, Iyunga 53119, Mbeya, Tanzania*

This study involves the use of friend-of-friend method on the volume limited samples constructed from the Sloan Digital Sky Survey Data Release 12 (SDSS DR12) to classify the galaxies into isolated and non-isolated environments hence to investigate the influence of the galaxy environment on the main sequence of star formation, and colour bimodality. We classified the galaxies into the luminous volume-limited sample with $-22.5 \leq M_r \leq -20.5$ (mag), and the faint volume-limited sample with $-20.5 \leq M_r \leq -18.5$ (mag). Using the WHAN diagnostic diagram we assigned the samples into star-forming, strong AGN, weak AGN, and retired galaxies based on their environment (isolated and non-isolated). The friend-of-friend method was successful in producing consistent results regarding the stellar mass-SFR and stellar mass-colour known relations. Apart from that the decrease in the slope of the main sequence for star-forming galaxies by 0.04 dex and intercept by 0.39 dex for the luminous sample was observed while the faint sample a decrease of 0.08 dex in slope and 0.74 dex in intercept was observed between isolated and non-isolated galaxies. A significant difference on the number of galaxies between isolated and non-isolated galaxies within, above and below the main sequence by 7.47%, 28.51%, 14.59% for the luminous sample while for the faint sample by 16.15%, 32.60%, 35.23% on average, respectively are observed. A significant difference in the number of galaxies in the blue cloud, green valley, and red sequence by 10.30%, 20.61%, 5.74% for luminous sample while for faint sample by 28.46%, 41.36%, 8.95% on average, respectively was observed. The study concludes that the galaxy environment influences the shaping and positioning of galaxies along the star formation main sequence and colour bimodality.

Keywords: Main sequence; Colour bimodality; Green valley; Galaxy environment.

I. INTRODUCTION

The star-forming (SF) main sequence (MS) refers to a close relationship between the rates at which stars are formed and the changes in the masses of stars (M_\star s) in the majority of the galaxy population undergoing star formation. The baseline of the correlation between these two parameters changes over time, indicating that the intensity of star formation changes significantly with time. A comprehensive understanding of how the MS evolves is crucial for capturing fundamental insights into how galaxies grow. In this regard, the slope of the correlation between the star formation rates (SFRs) and M_\star provides information on how star formation activity changes across diverse stellar masses, while the dispersion of this correlation unveils the degree of unpredictability in the history of gas accretion and the efficiency of star formation [1–7]. Therefore, comprehending the trajectory of galaxies over time in the SFR versus M_\star plane serves as a potential tool for identifying the processes responsible for the gradual decline in star formation activity as time progresses. There is considerable uncertainty in the literature regarding the slope and dispersion of this correlation. The predominant source of uncertainty arises from the biases introduced by various factors. These may include criteria employed in the sample selection, evolution of gas density with redshift and non-linearity of the relation, where the slope varies across different mass scales.

By selecting the SF galaxies from the seventh release of SDSS data [8] within the range of redshift $0.02 < z < 0.085$, Ref. [9] obtained the absence of deviation from the simple power-law MS relation in the local galaxies. This study revealed that the deviation originates from the inconsistency in SF galaxies' selection. However, in this study, the active galactic nucleus (AGN) galaxies were excluded from the analysis and only the SF galaxies were discussed. Further, it is believed that AGNs might be one possible cause for shifting their host galaxy's placement with respect to the MS [10]. Subsequent works by Refs. [11, 12] demonstrated that low-luminosity AGNs have SFRs that are below or on the MS and complimented the initial finding that galaxies hosting high-luminosity AGNs have enhanced SFRs compared to the MS. When studying the AGNs from MaNGA survey [13], Ref. [14] observed high-luminosity AGNs to have enhanced SFRs compared to the MS. On the other hand, Ref. [15] observed that using colour-colour selection method of SF galaxies results in a steep MS due to the exclusion of red dusty SF galaxies.

The normalization of the MS evolution is thought to be due to the evolution of gas density with redshift [1, 16–23]. There is an observation that the MS obeys the power law shape, $\text{SFR} \propto M_\star^\alpha$, both in the local Universe and distant Universe [1, 17]. Other works suggest that the SFR vs M_\star relation obeys a curvature nature towards the high mass at the low [18] and high redshift [15, 21–24]. Also, there is ongoing debate in the literature regarding the scatter around the relation having conflicting

* Email: privatuspius08@gmail.com

† Email: umananda2@gmail.com

results [20, 21, 25–31]. Some works, for example Ref. [25], report a constant scatter of 0.2–0.3 dex from low to moderate high masses. Some studies, for example, [26], report a decrease of scatter for the mass range ($10^8 \lesssim M_\star \lesssim 10^{10}/M_\odot$) at different redshift. Ref. [21], using the sample from CANDELS fields [27], within the stellar mass range ($8.4 \lesssim M_\star \lesssim 9.2/M_\odot$) at $0.5 \lesssim z \lesssim 2.5$, observed that the slope is dependent on stellar mass that is steeper at low masses than high masses. Ref. [28], using the data from the XMM-Spitzer Extragalactic Representative Volume Survey (XMM-SERVS) [29], observed that the less massive AGNs ($10^{9.5} \lesssim M_\star \lesssim 10^{10.5}/M_\odot$) possess enhanced SFR than when compared to normal galaxies, while more massive ($10^{10.5} \lesssim M_\star \lesssim 10^{11.5}/M_\odot$) one lie on or below the MS.

Moreover, the galaxy colour versus stellar mass which serves as a potential tool for identifying the mechanism deriving this bimodality is another very important subject to undertake [30, 32]. Different studies tried to include the AGNs in the colour versus stellar mass diagram and obtained that these galaxies populate the red sequence and the state between blue cloud and red sequence which is known as green valley. For example, Ref. [32] obtained that the inclusion of AGNs in these diagrams enables to obtain the role of AGNs feedback in the quenching of SFR of early-type galaxies. Ref. [33] obtained that the AGNs are populated on a distinct region of the colour versus stellar mass diagram referred to as the red sequence or top of the blue cloud, believing that a key stage in the massive galaxies’ evolution is the quenching of SFR at which there is the migration of the blue cloud to the red sequence. On the other hand Ref. [33] outlined that AGNs may be the cause for the decrease of SFR as time progresses, they outlined that the ongoing star formation is not a necessary condition for the AGN activity since the black holes’ accretions are observed when the star formation has been terminated. Ref. [34] observed morphology quenching to be a reason for the reduction of star formation activities in galaxies mainly as a bulge formation which stabilizes the gas disc against the gravitational instabilities.

Different literature tried to associate the decrease of SFR with the environment, for example Ref. [35], studying the radial profiles in $H\alpha$ equivalent width and specific star formation rate (SSFR) derived from spatially resolved MaNGA survey [13], to gain insight into the physical mechanisms that suppress star formation, observed that the responsible quenching mechanism appears to affect the entire galaxy. Ref. [36] obtained that morphology and environment have a combined role in slowing down the star formation activities in galaxies. Furthermore, they observed that a long-timescale environmental effect appears at low redshift. Ref. [37] suggested that the decrease of SFR is mainly due to internal and linked with bulge growth. However, the existence of the relation between morphology and density may provide a different turn in the relation of SFR, stellar mass and the environment where a particular galaxy resides. The study by Ref. [38], presenting the analysis of star formation and quenching in the SDSS MaNGA survey [13], utilizing over 5 million spaxels from ~ 3500 local galaxies, observed that the sudden decrease of SFR affect the whole galaxy but star formation occurs in a small localized scale within the galaxy. These studies aim to discern the mechanism or combination of mechanisms that lead to the quenching of star formation processes in galaxies, thereby influencing their evolution.

In a simplified representation, the process guiding these transformations can be broadly categorized as ‘internal’ and ‘external’. Rather than being driven by stochastic events like massive mergers and starbursts, Ref. [1] demonstrated that the normalization declines dramatically but steadily as a function of redshift, possibly on mass-dependent time scales. Keeping in mind that more precise the relation of redshift on evolution is often expressed as $\propto (1+z)^\gamma$, with γ which range from 1.9 to 3.7 [22–24]. Ref. [39], using the model of galaxy formation observed the AGN feedback to be the primary mechanism affecting the MS. Although this may affect the massive galaxies ($10^{11} M_\odot$), there is a lack of observed feedback effects for the majority of the SF galaxies [40]. However, Ref. [41] using a basic model for disk evolution, demonstrated that the evolution of galaxies away from the main sequence can be attributed to the depletion of gas due to star formation after a cut-off of gas inflow. This model was based on the observed dependence of star formation on gas content in local galaxies and assuming simple histories of cold gas inflow. Ref. [41] further obtained that Galaxies classified as MS, quiescent, or passive exhibit varying fractions on mass and environment. The MS fractions decrease with increasing mass and density, while the quiescent and passive fractions rise. Due to this uncertainty, the ongoing debate revolves around the extent to which each of these scenarios influences the shape of the relation.

In this paper, our primary goal is to investigate if, the star formation MS and that of colour– M_\star relation depends on the galaxy environment using isolated and non-isolated galaxy samples, derived using modified friend-of-friend algorithms by Ref. [42]. Our study tests if the method can produce the known facts in the literature regarding the relations, and quantifying the influence of the environment on the main sequence and colour bimodality. The width of the MS is defined as ± 0.3 dex ranging from the best-fit line of SFR– M_\star plane which was obtained based on the dispersion of the observed MS. This approach enables us to assess the linearity of the MS and explore the dispersion of the MS. Additionally, we aim to quantify the evolutionary trajectory of AGN, and retired galaxies with respect to the colour–stellar mass diagram, seeking insights into whether galaxy environment plays a role in shaping galaxy colour bimodality.

The structure of this paper is as follows. In the next section, we explain the source of data and the method of getting samples, in Section III we explain the methodology used in this study, Section IV is dedicated to presenting the results. In Section V the results are discussed. Section VI presents the summary and conclusion. Cosmological constants are adopted from Ref. [43], wherein the dark energy density parameter $\Omega_\Lambda = 0.692$, Hubble constant of $H_0 = 67.8 \text{ km s}^{-1} \text{ Mpc}^{-1}$ and the matter density parameter $\Omega_m = 0.308$ are recorded.

II. DATA

A. The SDSS main sample

In this research work the catalogue data extracted from the flux-limited sample of twelve releases of Sloan Digital Sky Survey (SDSS DR12) as detailed in Refs. [44, 45] are used. The main galaxy sample was selected from the main contiguous area of the survey based on the methods outlined in Ref. [42]. Galaxy data were downloaded from the SDSS Catalogue Archive Server (CAS). The objects with the spectroscopic class GALAXY or QSO [45] was selected as suggested by the SDSS team. We then filtered out galaxies with the galactic-extinction-correction based on Ref. [46] where Petrosian r-band magnitude fainter than 17.77 are rejected keeping in mind that the SDSS is incomplete at fainter magnitudes [47]. After correcting the redshift for the motion with respect to the cosmic microwave background (CMB), using the simplified formula $z_{\text{CMB}} = z_{\text{obs}} - v_p/c$, where v_p is a motion along the line of sight relative to the CMB, the upper distance limit at $z = 0.2$ was set. The final data set contains 584449 galaxies.

B. The volume-limited samples

As is already stated, the SDSS main data are flux-limited. One of the disadvantage of using the flux-limited sample is that only the luminous objects have a chance to be observed at large distances. Due to this problem the volume-limited samples are desired and hence we constructed a volume limited sample for uniformity in the sample. Due to the peculiar velocities of galaxies in groups, the measured redshift (recession velocity) does not give an accurate distance to a galaxy located in a group or cluster, and hence to overcome this issue the apparent magnitude was transformed into absolute magnitude using the relation:

$$M_r = m_r - 25 - 5 \log_{10}(d_L) - K, \quad (1)$$

where d_L is the luminosity distance, M_r and m_r are r-band absolute and apparent magnitudes respectively, and K is the k+e-correction. The k-corrections were calculated with the KCORRECT (*v4.2*) algorithm [48]. The evolution corrections were estimated using the luminosity evolution model of $K_e = cz$, where $z = -1.62$ for the r-filter [49]. The magnitudes correspond to the rest-frame (at the redshift $z = 0$) and the evolution correction was estimated similarly by assuming a distance-independent luminosity function [50, 51].

According to Ref. [52], the Schechter function's [53] typical magnitude M_r^* is around -20.5 mag. The physical properties of galaxies have been shown to undergo an abrupt transition at the typical magnitude M_r^* . The variation in the clustering amplitude of galaxies with the absolute magnitude or the galaxy luminosity's environmental dependency is relatively weak for galaxies fainter than M_r^* , but rather strong for those brighter [54]. In order to better explore the galaxy properties, it is interesting to compare the two types of galaxies as described above. We have constructed the volume-limited samples below and above the characteristic magnitude M_r^* by calculating the effective maximum distance using the relation as given by

$$d_{\text{max}} = 10^{(m_{r\text{lim}} - M_{r\text{min}} + 5)/5} \times 10^{-6} (\text{Mpc}), \quad (2)$$

where $m_{r\text{lim}} = 17.17$ mag, $M_{r\text{min}} = -20.5$ mag for luminous and $M_{r\text{min}} = -18.5$ mag for faint samples, respectively. Using the d_{max} values and the luminosity restrictions we constructed the luminous volume-limited main galaxy sample contains 136274 galaxies with $-22.5 \leq M_r \leq -20.5$ (mag), and the faint volume-limited sample, contains 26513 galaxies with $-20.5 \leq M_r \leq -18.5$ (mag).

III. METHODOLOGY

A. Isolated and non-isolated environment

For each volume-limited sample, we assigned the galaxies into isolated and non-isolated sub-samples, compiled using the friend-of-friend (FoF) method with a variable linking length. The essence of this approach lies in the division of the sample into distinct systems through an objective and automated process. This involves creating spheres with a linking length (R) around each sample point (galaxy). To adjust the linking length based on distance, the procedures outlined in Ref. [42] were applied. The relationship between the linking length and the redshift is represented by an arctangent law as given by

$$R_{LL}(z) = R_{LL,0} [1 + a \arctan(z/z_*)], \quad (3)$$

where $R_{LL}(z)$ is the linking length used to create a sphere at a specific redshift, $R_{LL,0}$ is the linking length at $z = 0$, a and z_* are free parameters. The values of $R_{LL,0} = 0.34$ Mpc, $a = 1.4$ and $z_* = 0.09$ are obtained by fitting equation (3) to the

linking length scaling relation. If there are other galaxies within the sphere, they are considered as parts of the same system and referred to as ‘friends’. Subsequently, additional spheres are drawn around these newly identified neighbours, and the process continues with the principle that ‘any friend of my friend is my friend’. This iterative procedure persists until no new neighbours or ‘friends’ can be added. At that point, the process concludes and a system is defined. The galaxies in the system with no neighbour ($N_{gal} = 1$) are isolated, while the galaxies with more than one neighbour ($N_{gal} \geq 2$) are non-isolated. Consequently, each system comprises isolated galaxies or non-isolated galaxies that share at least one neighbour within a distance not exceeding R . For the luminous volume-limited main galaxy sample a total of 58038(42.59%) isolated and 78233(57.41%) non-isolated galaxies were obtained, while for faint volume-limited main galaxy sample a total of 10659(40.20%) isolated and 15854(59.80%) non-isolated galaxies were obtained.

B. Galaxy properties

The stellar masses used in this study were obtained from the Max Planck Institute for Astrophysics and Johns Hopkins University (MPA-JHU) team, calculated from the Bayesian approach as detailed in Ref. [55]. The Stellar mass calculation within the SDSS spectroscopic fiber aperture relies on the fiber magnitudes, whereas the total stellar mass is determined using the model magnitudes.

The MPA-JHU total SFR used in this study was derived from the MPA-JHU database and estimated using the methods of Refs. [56, 57] with adjustments made for the non-SF galaxies. The MPA-JHU team uses the $H\alpha$ calibration [58] to determine the SFR for galaxies classed as SF. In contrast to the approach taken by Ref. [56], the MPA-JHU team applied aperture corrections for SFR by fitting the photometric data from the outer regions of the galaxies. Specifically, for the SFR computation, Ref. [56] outlined the calculation within the galaxy fiber aperture. It is important to keep in mind that the region beyond the fiber SFR is estimated using the methods of Ref. [59]. Furthermore, for the case of AGN and weak emission line galaxies, SFR was determined using photometry. Keeping in mind that for the case of non-SF galaxies, the ionization originates from other sources, such as rejuvenation in the outer regions, post-AGB stars, or ionization from AGN. As such, the SFR based on $H\alpha$ for non-SF galaxies need to be regarded as a maximum value [60].

C. Galaxy classification

We classified the galaxies based on $W_{H\alpha}$ versus $[\text{NII}]/H\alpha$ (WHAN) diagram [61], where $W_{H\alpha}$ is the $H\alpha$ equivalent width, and $[\text{NII}]/H\alpha$ is the ratio of the $[\text{NII}]$ emission line to the $H\alpha$ line. From this diagram we can have following four inequalities [61]:

$$\log\left(\frac{[\text{NII}]}{H\alpha}\right) < -0.4 \quad \text{and} \quad W_{H\alpha} > 3 \text{ \AA}, \quad (4)$$

$$\log\left(\frac{[\text{NII}]}{H\alpha}\right) > -0.4 \quad \text{and} \quad W_{H\alpha} > 6 \text{ \AA}, \quad (5)$$

$$\log\left(\frac{[\text{NII}]}{H\alpha}\right) > -0.4 \quad \text{and} \quad 3 \text{ \AA} < W_{H\alpha} < 6 \text{ \AA}, \quad (6)$$

$$W_{H\alpha} < 3 \text{ \AA}. \quad (7)$$

These inequalities (4), (5), (6) and (7) represent the pure SF galaxies, strong AGN, weak AGN and retired galaxies (RGs), respectively [61]. The use of WHAN diagram is to increase the accuracy of our analysis, due to the factor that the usual traditional diagnostic diagrams (BPT) of Refs. [32, 62–64] may introduce bias since it is well known that shock ionization and AGNs could cover almost any region between the right-bottom end of the loci (usually assigned to SF regions) up to the top-right end of the diagram. On the other hand Low Ionization -Nuclear- Emission line Region (LINER) used in BPT diagram may contain possible multiple ionizing sources [61, 65–67].

The distribution of galaxies is shown in Fig. 1, wherein the SF galaxies are shown in blue colour, strong AGNs in red colour, weak AGNs in green colour and RGs in cyan colour. In the luminous volume-limited sample, the following numbers are obtained, for isolated galaxies: 18259 (31.46%) SF galaxies; 13231 (22.80%) strong AGNs; 5199 (8.96%) weak AGNs and 21349 (36.78%) RGs, while for non-isolated sample: 17145 (21.91%) SF galaxies; 14447 (18.47%) strong AGNs; 6837 (8.74%) weak AGNs and 39807 (50.88%) RGs. In the faint volume-limited sample, the following numbers are obtained, for isolated galaxies: 8406 (78.86%) SF galaxies; 841 (7.89%) strong AGNs; 370 (3.47%) weak AGNs and 1042 (9.78%) RGs, while for non-isolated sample: 10157 (64.07%) SF galaxies; 1205 (7.60%) strong AGNs; 751 (4.74%) weak AGNs and 3741 (23.60%) RGs.

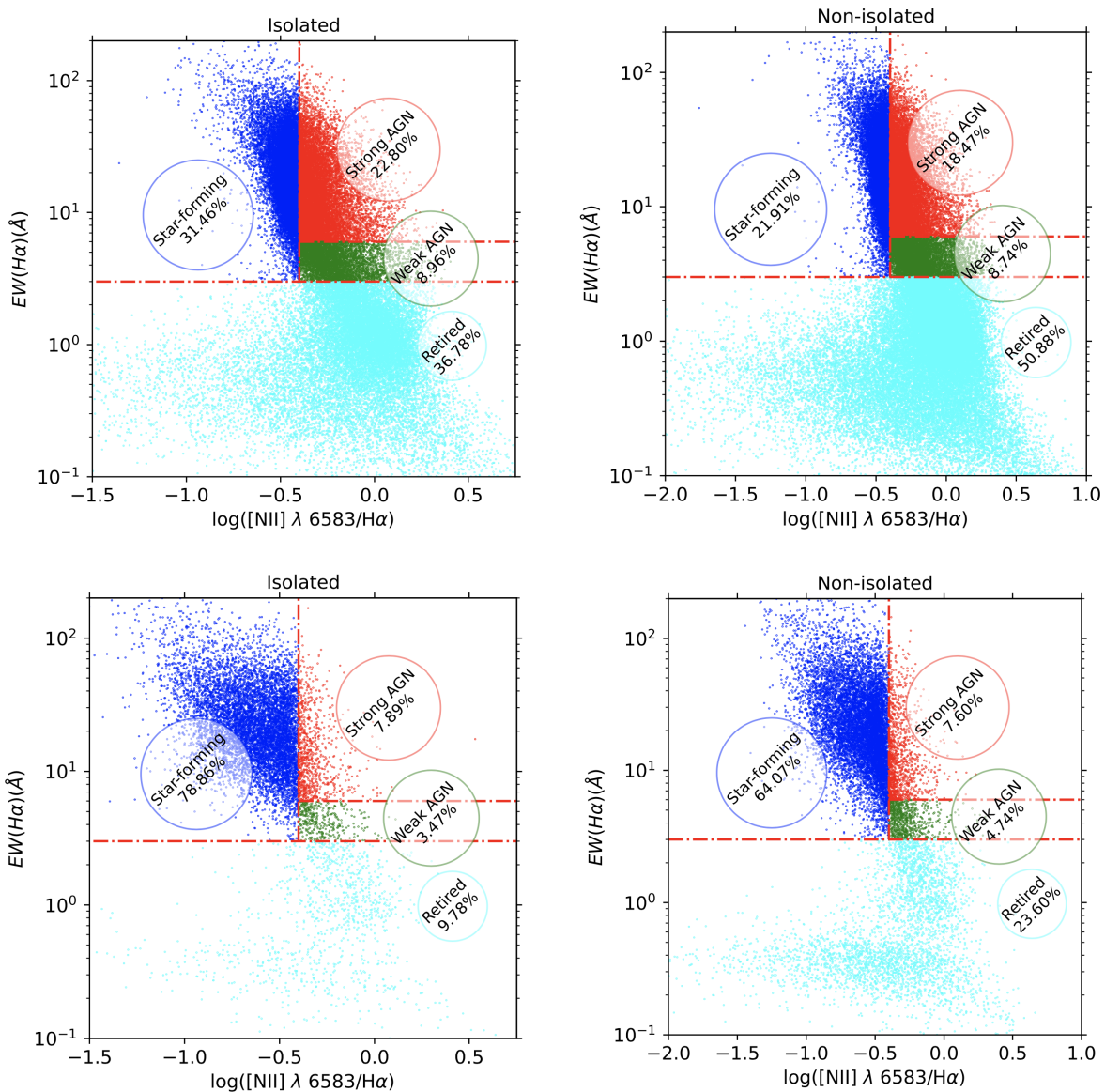


FIG. 1. WHAN diagrams for the luminous volume limited main galaxy sample (upper panels) and faint volume-limited main galaxy sample (lower panels) with isolated (left panels) and non-isolated (right panels) samples.

IV. RESULTS

A. The Main Sequence (MS)

The equation of the MS for SF galaxies shows a tight relationship between the $\log(\text{SFR})$ and $\log(M_*)$, which has been studied in a number of works [1, 25, 30, 32, 68–70]. The relationship serves as the tracer on how the stars are formed in relation to the stellar mass within a galaxy. The MS is generally characterized by such a relation as given by

$$\log_{10}(\text{SFR}) = \beta \log_{10}(M_*) + \alpha, \quad (8)$$

where β and α are slope and intercept, respectively. Aiming at studying how the environment affects the SFR relative to the M_* for the SF, strong AGN, weak AGN, retired classified sub-samples of galaxies, we generate the equation of the best-fitted line of the SF galaxies (the equation of MS based on Eq. (8)). This best-fitted line is used as a reference to understand the behaviour of SFR relative to M_* for all other sub-samples of galaxies residing in different environments. Fig. 2 shows the distributions of SFR with respect to M_* of the SF, strong AGN, weak AGN and retired galaxies for isolated and non-isolated cases along with

the corresponding best-fitted MS line of the SF galaxies. The width of the MS of $\sim \pm 0.3$ dex (dashed lines) in the plots of this figure as already stated is selected based on the dispersion of the observed MS. The figures show the positions of galaxies for all sub-samples with respect to the MS and the corresponding numbers of galaxies with their percentages are shown in Table I for the luminous, and in Table II for the faint volume-limited sample. By performing the regression analysis for the luminous

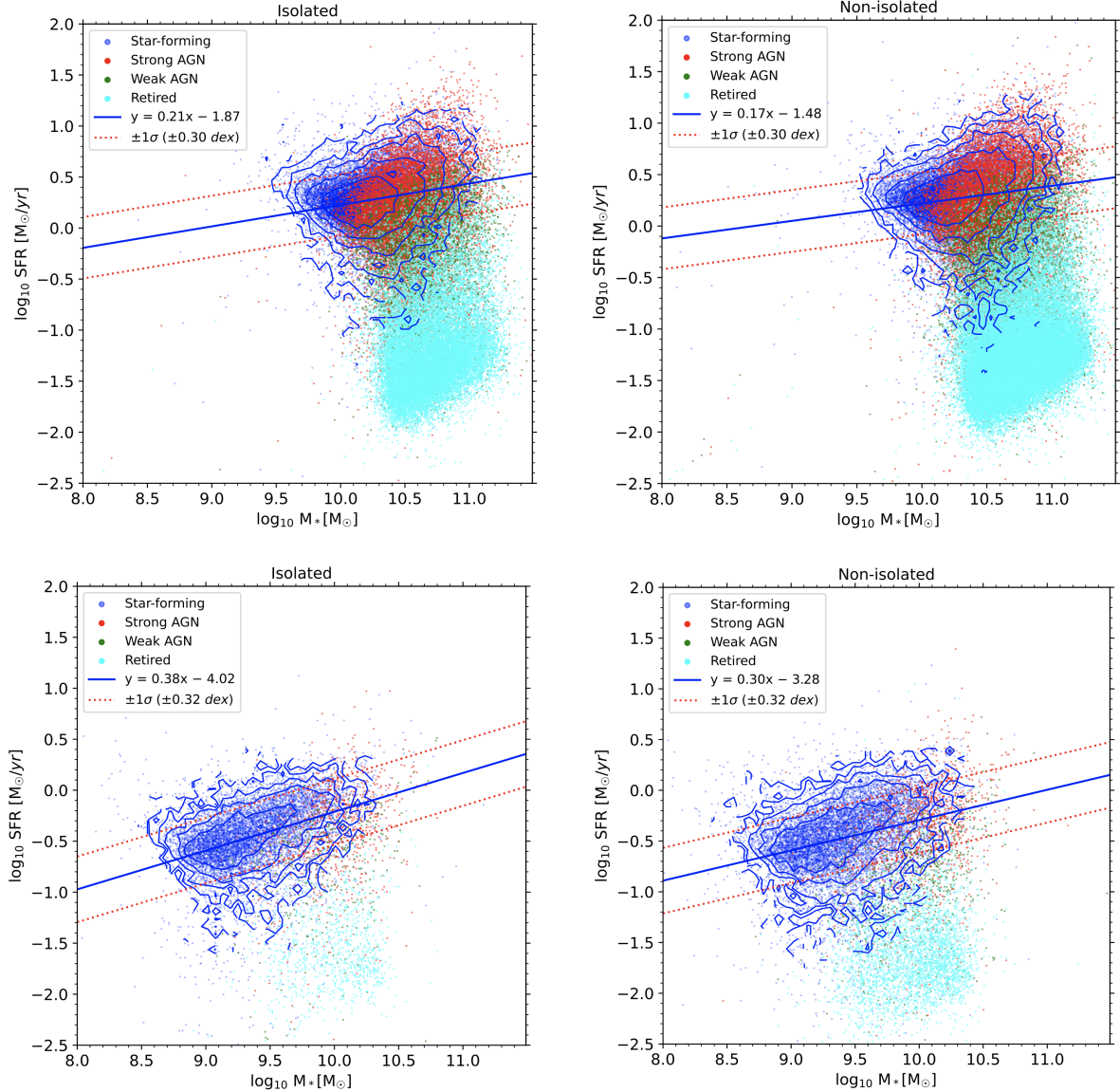


FIG. 2. Scatter plot showing the SFR as the function of stellar mass for the luminous volume-limited main galaxy sample (upper panels) and the faint volume-limited main galaxy sample (lower panels) with isolated (left panels) and non-isolated (right panels) SF (blue with contour plot), Strong AGN (red points), weak AGN (green points) and retired (cyan points) galaxies. The width of the MS on each diagram correspond to the standard deviation ($\pm 1\sigma$) representing the scatter around the MS ($\sim \pm 0.3$ dex).

volume limited sample the general equations of the best-fitted line for the isolated and non-isolated galaxies are respectively given by Eqs. (9) and (10).

$$\log_{10}(\text{SFR}) = 0.21 \pm 0.01 \log_{10}(M_{\star}) - 1.87 \pm 0.10, \quad (9)$$

$$\log_{10}(\text{SFR}) = 0.17 \pm 0.01 \log_{10}(M_{\star}) - 1.48 \pm 0.10. \quad (10)$$

Similarly, for the faint volume-limited sample the general equations of the the best-fitted line for the isolated and non-isolated galaxies are respectively given by Eqs. (11) and (12).

$$\log_{10}(\text{SFR}) = 0.38 \pm 0.01 \log_{10}(M_*) - 4.02 \pm 0.10, \quad (11)$$

$$\log_{10}(\text{SFR}) = 0.30 \pm 0.01 \log_{10}(M_*) - 3.28 \pm 0.10. \quad (12)$$

The associated errors in Eqs. (9), (10), (11) and (12) are the standard deviations in the slope and intercept. Table III indicates the percentage difference between isolated and non-isolated galaxies for the luminous sample above MS, within MS and below MS for SF (column 2), Strong AGN (column 3), Weak AGN (column 4) and retired (column 5) galaxies, while for the faint sample SF (column 6), Strong AGN (column 7), Weak AGN (column 8) and retired (column 9) galaxies, respectively. This table can be used as the tracer on how the positioning of galaxies in the plane of SFR versus M_* are affected by environment.

TABLE I. Number of galaxies within (MS), above (Above MS), and below (Below MS) the star-forming main sequence for isolated (iso) and non-isolated (nis) environments for the luminous volume-limited sample.

Position (1)	Star-forming (%)		Strong AGN (%)		Weak AGN(%)		Retired (%)	
	iso (2)	nis (3)	iso (4)	nis (5)	iso (6)	nis (7)	iso (8)	nis (9)
MS	14480(79.30)	12883(75.14)	7682(58.06)	7819(54.12)	1362(26.20)	1522(22.26)	452(2.12)	645(1.62)
Above MS	1963(10.75)	2216(12.93)	1369(10.35)	1918(13.28)	18(0.35)	38(0.56)	10(0.05)	35(0.09)
Below MS	1816(9.95)	2046(11.93)	4180(31.59)	4710(32.60)	3819(73.46)	5277(77.18)	20887(97.83)	39127(98.29)
Total	18259(100)	17145(100)	13231(100)	14447(100)	5199(100)	6837(100)	21349(100)	39807(100)

TABLE II. Number of galaxies within (MS), above (Above MS), and below (Below MS) the star-forming main sequence for isolated (iso) and non-isolated (nis) environments for the faint volume limited sample.

Position (1)	Star-forming (%)		Strong AGN (%)		Weak AGN (%)		Retired (%)	
	iso (2)	nis (3)	iso (4)	nis (5)	iso (6)	nis (7)	iso (8)	nis (9)
MS	6416(76.33)	7018(69.10)	515(61.24)	660(54.77)	146(39.46)	193(25.70)	39(3.74)	79(2.11)
Above MS	995(11.84)	1626(16.01)	70(8.32)	165(13.69)	9(2.43)	8(1.07)	2(0.19)	8(0.21)
Below MS	995(11.84)	1513(14.90)	256(30.44)	380(31.54)	215(58.11)	550(73.24)	1001(96.07)	3654(97.68)
Total	8406(100)	10157(100)	841(100)	1205(100)	370(100)	751(100)	1042(100)	3741(100)

TABLE III. The percentage difference (Δ (%)) of isolated and non-isolated galaxies within MS, above MS and below MS.

Position (1)	Luminous Δ (%)					Faint Δ (%)				
	Star-forming (2)	Strong AGN (3)	Weak AGN (4)	Retired (5)	Average (6)	Star-forming (7)	Strong AGN (8)	Weak AGN (9)	Retired (10)	Average (11)
MS	5.84	0.88	5.55	17.59	7.47	4.48	12.34	13.86	33.90	16.15
Above MS	6.05	16.70	35.71	55.56	28.51	24.07	40.43	5.88	60.00	32.60
Below MS	5.96	5.96	16.03	30.39	14.59	20.65	19.50	43.79	56.99	35.23

B. Colour Bimodality

Galaxies can be categorized into two groups: those actively forming stars, appearing blue, and those lacking significant star formation, appearing red. The galaxies initially fall into the blue sub-category and then they change gradually to red [71, 72]. It is clear to say that evolution from one category to another must involve processes which quench their rate of forming new stars

from the blue cloud passing the intermediate stage (green valley) to the red sequence [73, 74]. The factors for this transformation may be due to internal mechanisms like negative feedback from the AGNs and the galaxy environment. To study the effect of the environment on colour, Table IV shows the number of galaxies with respect to the green valley (GV) for the luminous samples, while Table V shows the number of galaxies with respect to the GV for the faint sample, respectively. The position of galaxies on the colour against the stellar mass diagram is shown in Fig 3 for the SF, strong AGN, and weak AGN and retired galaxies respectively. The width of the GV is derived following the Ref. [75], which is obtained from equations,

$$u - r = -0.24 + 0.25 \times M_{\star}, \quad (13)$$

$$u - r = -0.75 + 0.25 \times M_{\star}. \quad (14)$$

Here u and r magnitudes were derived from the SDSS database with extinction corrected. Table VI indicates the percentage change of colour between isolated and non-isolated galaxies for the luminous sample above GV, within GV and below GV for SF (column 2), Strong AGN (column 3), Weak AGN (column 4) and retired (column 5) galaxies, while for the faint sample SF (column 6), Strong AGN (column 7), Weak AGN (column 8) and retired (column 9) galaxies, respectively. This table can be used to trace how the positioning of galaxies in the colour against the stellar mass diagram is affected by changing the galaxies' environment.

TABLE IV. Number of galaxies within the green valley (GV), above the green valley (Above GV) and below the green valley (Below GV) for isolated (iso) and non-isolated (nis) galaxies for the luminous volume-limited sample.

Position (1)	Star-forming (%)		Strong AGN (%)		Weak AGN (%)		Retired (%)	
	iso (2)	nis (3)	iso (4)	nis (5)	iso (6)	nis (7)	iso (8)	nis (9)
GV	5023(27.51)	5360(31.26)	7302(55.19)	8015(55.48)	2854(54.90)	3560(52.07)	5606(26.26)	8819(22.15)
Above GV	881(4.83)	1085(6.33)	1872(14.15)	2443(16.91)	1494(28.74)	2512(36.74)	15123(70.84)	30303(76.12)
Below GV	12355(67.67)	10700(62.41)	4057(30.66)	3989(27.61)	851(16.37)	765(11.19)	620(2.90)	685(1.72)
Total	18259(100)	17145(100)	13231(100)	14447(100)	5199(100)	6837(100)	21349(100)	39807(100)

TABLE V. Number of galaxies within the green valley (GV), above the green valley (Above GV) and below the green valley (Below GV) for isolated (iso) and non-isolated (nis) galaxies for the faint volume-limited sample.

Position (1)	Star-forming (%)		Strong AGN (%)		Weak AGN (%)		Retired (%)	
	iso (2)	nis (3)	iso (4)	nis (5)	iso (6)	nis (7)	iso (8)	nis (9)
GV	2863(34.06)	3874(38.14)	513(61.00)	710(58.92)	202(54.59)	374(49.80)	245(23.51)	794(21.22)
Above GV	615(7.32)	1026(10.10)	171(20.33)	334(27.72)	109(29.46)	328(43.68)	774(74.28)	2911(77.82)
Below GV	4928(58.62)	5257(51.76)	157(18.67)	161(13.36)	59(15.95)	49(6.52)	23(2.21)	36(0.96)
Total	8406(100)	10157(100)	841(100)	1205(100)	370(100)	751(100)	1042(100)	3741(100)

TABLE VI. Percentage difference (Δ (%)) of isolated and non-isolated galaxies within the green valley (GV), above the green valley (Above GV) and below the green valley (below GV) for luminous and faint samples.

Position (1)	Luminous Δ (%)					Faint Δ (%)				
	Star-forming (2)	Strong AGN (3)	weak AGN (4)	Retired (5)	Average (6)	Star-forming (7)	Strong AGN (8)	weak AGN (9)	Retired (10)	Average (11)
GV	3.25	4.65	11.01	22.27	10.30	15.01	16.11	29.86	52.84	28.46
Above GV	10.38	13.23	25.41	33.42	20.61	25.05	32.28	50.11	57.99	41.36
Below GV	7.18	0.85	4.98	9.96	5.74	3.23	1.26	9.26	22.03	8.95

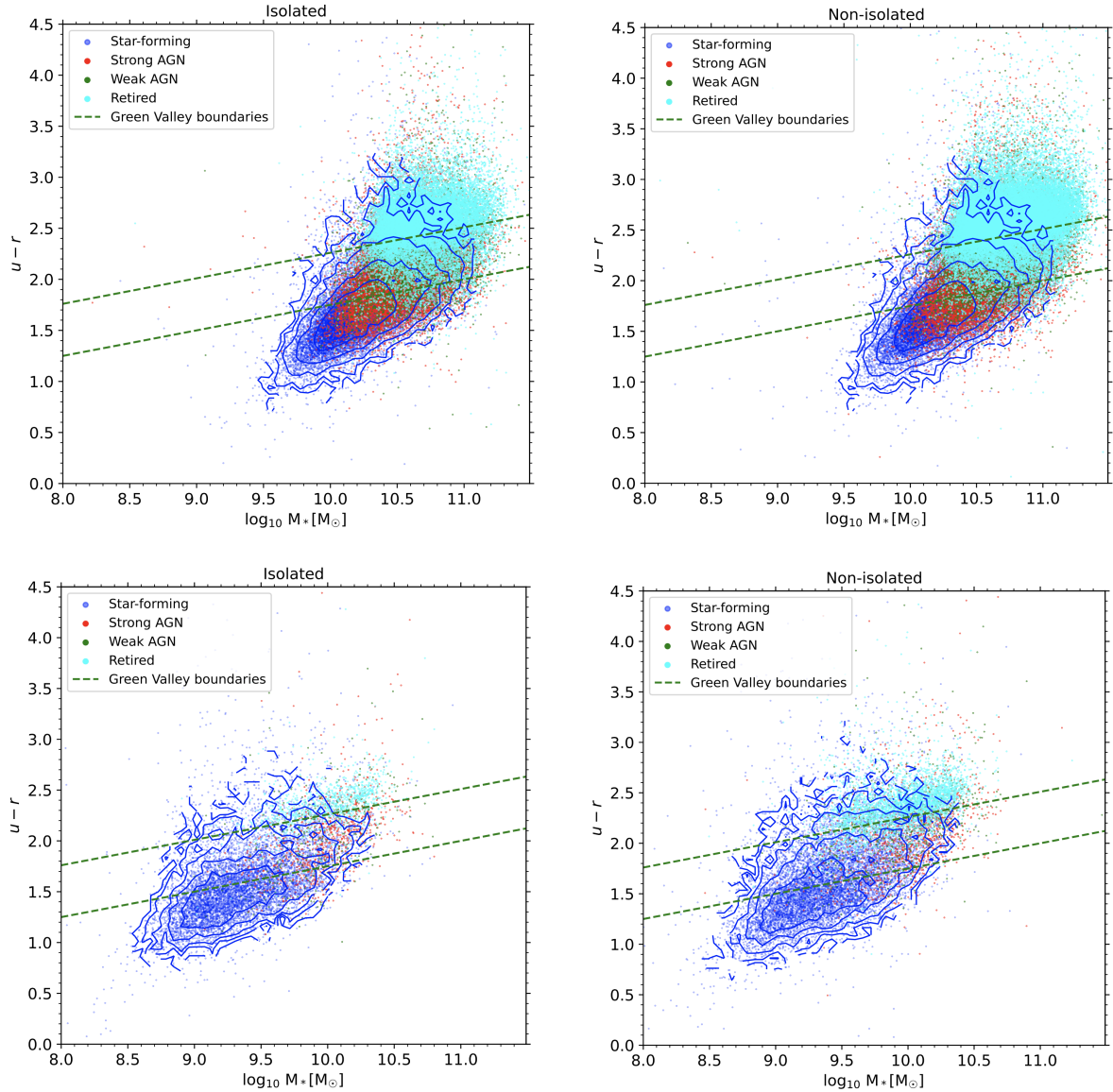


FIG. 3. Distribution of galaxy's rest-frame colour against stellar mass for the luminous volume-limited main galaxy sample (upper panels) and the faint volume-limited main galaxy sample (lower panels) with isolated (left panels) and non-isolated (right panels) galaxies including SF (blue with contour plots), strong AGN (red points), weak AGN (green points) and retired (cyan points).

V. DISCUSSION

From Fig 1 it is observed that the fraction of SF galaxies for the faint volume-limited sample is always larger than the luminous volume-limited sample for both isolated and non-isolated galaxies. For luminous galaxies, the fraction of RGs is larger than SF, strong AGN, and weak AGN, while for the faint volume-limited sample the fraction of star-forming galaxies are larger than strong AGN, weak AGN, and retired galaxies. In the luminous volume-limited sample, the difference in the fraction of galaxies between isolated and non-isolated galaxies are 3.15%, 4.39%, 13.61, 30.18% for SF, strong AGN, weak AGN, and retired galaxies, respectively. In the faint sample, the difference in fractions are 9.43%, 17.79%, 33.99%, 56.43% for SF, strong AGN, weak AGN, and retired galaxies, respectively. Again from Fig 1, we observe that the fraction of isolated strong AGN for both luminous and faint volume-limited samples is always larger than the non-isolated sample. Since the non-isolated environment is observed to be an area of high density our study agrees with Ref. [76], which studied the AGNs and observed that the fraction of low-density AGNs is larger than the sample of higher-density AGNs.

From Fig 2, the difference of 0.04 dex in slope, and 0.39 dex in intercept between the isolated and non-isolated luminous volume-limited samples are observed, while for the faint volume-limited sample a difference of 0.08 dex in slope and 0.74 dex

in intercept is observed. Using two samples t-statistics test P-values of 7.19×10^{-4} , 1.16×10^{-3} for the luminous sample and 8.78×10^{-10} , 3.97×10^{-9} for the faint sample in slope, intercept respectively, were obtained indicating that the observed differences in slope and intercept for both luminous and faint sample are statistically significant. From the equations of star formation MS, it is observed that the slope of the isolated galaxies is greater than non-isolated galaxies. This originated from the fact that the SFR decreases for non-isolated galaxies while stellar mass increases when the galaxies are with companions. These results support the findings of Refs. [25, 77–83], regarding fluctuations in SFR with environment. On the other hand, the luminous volume-limited samples possess lower slopes than the faint volume-limited samples for both isolated and non-isolated galaxies this indicates that the faint galaxies possess higher SFR and lower masses than the luminous volume-limited sample. Again from Fig 2 the stellar mass is observed to increase following the sequence SF, strong AGN, weak AGN and retired galaxies. The SFR decreases in the same sequence, agreeing with the findings by Ref. [54] which observed that galaxies hosting AGNs are preferentially more massive and have low SFR. The study is consistent with the results from Ref. [60] which presented a characterization of the primary characteristics of a sample of 98 AGN host galaxies, both type-II and type-I. They found that, on average, AGN hosts are more massive and more compact than SF galaxies, compared with those of $\simeq 2700$ non-active galaxies observed by the MaNGA survey.

The increase of 0.17 dex and 2.15 dex in slope and intercept respectively is observed between the isolated luminous and the isolated faint volume-limited samples, while the increase of 0.13 dex in slope and 1.8 dex in intercept is observed between non-isolated luminous and faint volume-limited samples indicating that luminosity is another very an important factor shaping the MS, where the effect is significant for the isolated than the non-isolated galaxies. From Table I and II, it is observed that there is a difference in fractions between isolated and non-isolated galaxies for SF, strong AGN, weak AGN and retired galaxies as shown by Table III, where for the luminous sample the differences of the number of galaxies within, above and below the main sequence are respectively 7.47%, 28.51%, 14.59%, while for the faint sample the differences are 16.15%, 32.60%, 35.23% on average, respectively. This differences produce an average P-values of 8.37×10^{-10} , 2.48×10^{-3} , 4.13×10^{-3} , 3.44×10^{-3} for the luminous sample and 4.89×10^{-10} , 2.12×10^{-3} , 4.44×10^{-3} , 3.37×10^{-3} for the faint sample under a two-sample chi-square statistical test (χ^2) for SF, strong AGN, weak AGN, and retired galaxies, respectively. These P values are much less than the standard value in statistics (0.05), indicating that the differences are statistically significant supporting the evidence from Refs. [11, 12, 14, 28], regarding the positioning of galaxies with respect to the main sequence.

From Table IV and V, it is observed that there is a difference in fraction between isolated and non-isolated galaxies for SF, strong AGN, weak AGN and retired galaxies as shown by Table VI, indicating that position of galaxies with respect to the green valley is affected by the environment for both luminous and faint volume galaxy samples. The difference of the number of galaxies within, above and below the green valley by 10.30%, 20.61%, 5.74% for the luminous sample while for the faint sample by 28.46%, 41.36%, 8.95% on average, respectively is observed. These differences produce an average P-value of 2.59×10^{-10} , 2.12×10^{-3} , 7.40×10^{-4} , 2.12×10^{-22} for the luminous sample and 3.13×10^{-9} , 1.24×10^{-3} , 4.93×10^{-4} , 4.79×10^{-4} for the faint sample under a two-sample chi-square statistical test (χ^2) for SF, strong AGN, weak AGN, and retired galaxies respectively. These P-values indicate that the differences are statistically significant which means there is a significant difference in the number of galaxies in blue cloud, green valley and the red sequence between isolated and non-isolated environments. Hence the galaxy environment influences colour bimodality. The u-r colour against M_* diagrams in Fig. 3, reinforces the relation with respect to the MS in Eq (8), the strong AGN galaxies are more redder and more massive than the SF, the weak AGN galaxies are more massive and redder than strong AGN, and retired have the highest stellar mass and most redder. These observations are consistent with the results of Ref. [30], which found that the SF was blue in colour and had lower masses. The larger fraction of galaxies within and above the GV in Tables V and IV show that the non-isolated environment accelerates the rate of change in SFR in comparison to the isolated environment. Furthermore, the lower fraction of the number of galaxies below the green valley for non-isolated galaxies when compared to isolated galaxies indicates the decrease of SFR for non-isolated galaxies. From Fig. 3, it is observed that the SF galaxies form a blue cloud since most of the galaxies are below the green valley as revealed by Table IV and V, where $\sim 60\%$ of SF are below the main sequence. Strong AGN are in a green valley as most of the galaxies lie within the demarcation lines ($\sim 58\%$) on average. Furthermore, it indicates that most of weak AGN galaxies galaxies are within the green valley ($\sim 53\%$) on average and retired galaxies are above the green valley ($\sim 75\%$) on average. These results are consistent with Ref. [84], wherein it is observed that the AGN hosts are found in transitory parts (i.e., green-valley) in almost all analysed properties which present bimodal distributions, using 867 galaxies extracted from the extended Calar-Alto Legacy Integral Field spectroscopy Area (eCALIFA) [85]. Similar to this, the study by Ref. [60] found that AGNs are situated in the ‘green valley’, the transition area between SF and non-SF galaxies, and they hypothesized that this star formation is in the process of halting or quenching.

VI. SUMMARY AND CONCLUSION

For the first time we use the friend-of-friend method as detailed in Ref. [42] to study the dependence of star formation MS and colour bimodality on the environment. Using the flux limited sample from Sloan Digital Sky Survey as detailed in Refs. [44, 45], we constructed the volume-limited samples of luminous and faint galaxies. The galaxies were classified into

two systems within a specific radius. The galaxies with no companion are termed isolated while the one with more than one neighbour in a system are termed non-isolated. Using the WHAN diagram we classified the galaxies into SF, strong AGN, weak AGN, and retired galaxies. We used the stellar mass and SFR retrieved from MPA-JHU obtained using the methods outlined in Ref. [56, 57], to include the strong AGN, weak AGN and retired galaxies on the local star formation MS and colour, stellar mass diagram, then we study the influence of isolated and non-isolated environments on the star formation MS, and colour bimodality. The friends-of-friends method produced a consistent results with the previous studies obtained by different methods [1, 11, 12, 14, 28, 30, 60, 76, 82–84]. Apart from that our study revealed the following:

- The decrease of the slope for the MS of SF galaxies by 0.04 dex and intercept by 0.39 dex for the luminous volume limited sample, while for the faint volume-limited sample a decrease of 0.08 dex in slope, and 0.74 dex in intercept are observed between isolated and non-isolated galaxies. The differences produced a P-value of 7.19×10^{-4} , 1.16×10^{-3} for the luminous sample and 8.78×10^{-10} , 3.97×10^{-9} for the faint sample in slope and intercept, respectively proving that the difference is statistically significant implying that the environment is among the factors which contribute to the shaping of the star formation main sequence.
- A significant difference in the number of galaxies between isolated and non-isolated environment within, above and below the main sequence by 7.47%, 28.51%, 14.59% for the luminous and by 16.15%, 32.60%, 35.23% for faint samples on average, respectively are observed indicating that the environment influence the positioning of galaxies along the star formation MS.
- For colour bimodality a significant difference in the number of galaxies within, above and below the green valley by 10.30%, 20.61%, 5.74% for the luminous sample and by 28.46%, 41.36%, 8.95% for the faint sample on average, respectively between isolated and non-isolated galaxies are observed which implies that colour bimodality is influenced by the galaxy's environment.

In the next study (in preparation), as the follow-up of this work, we aim to investigate if ageing and quenching processes are influenced by the environment using the same method.

ACKNOWLEDGEMENTS

PP acknowledges support from The Government of Tanzania through the India Embassy, Mbeya University of Science and Technology (MUST) for Funding. UDG is thankful to the Inter-University Centre for Astronomy and Astrophysics (IUCAA), Pune, India for the Visiting Associateship of the institute. Funding for SDSS- III has been provided by the Alfred P. Sloan Foundation, the Participating Institutions, the National Science Foundation, and the U.S. Department of Energy Office of Science. The SDSS-III website is <http://www.sdss3.org/>. SDSS-III is managed by the Astrophysical Research Consortium for the Participating Institutions of the SDSS-III Collaboration including the University of Arizona, the Brazilian Participation Group, Brookhaven National Laboratory, Carnegie Mellon University, the University of Florida, the French Participation Group, the German Participation Group, Harvard University, the Instituto de Astrofísica de Canarias, the Michigan State/Notre Dame/JINA Participation Group, Johns Hopkins University, Lawrence Berkeley National Laboratory, Max Planck Institute for Astrophysics, Max Planck Institute for Extraterrestrial Physics, New Mexico State University, New York University, Ohio State University, Pennsylvania State University, University of Portsmouth, Princeton University, the Spanish Participation Group, University of Tokyo, the University of Utah, Vanderbilt University, the University of Virginia, the University of Washington, and Yale University.

-
- [1] J. Speagle, C. Steinhardt, P. Capak, J. Silverman et al. *A Highly Consistent Framework for the Evolution of the Star-Forming” Main Sequence” from $z \sim 0 - 6$* , *ApJS* **214**, 15 (2014) [arXiv:1405.2041].
- [2] P. Behroozi, R. Wechsler, C. Conroy, *The average star formation histories of galaxies in dark matter halos from $z \sim 0 - 8$* , *ApJ* **770**, 57 (2013) [arXiv:1207.6105].
- [3] K. Noeske, B. Weiner, S. Faber, C. Papovich et al. *Star formation in aegis field galaxies since $z= 1.1$: The dominance of gradually declining star formation, and the main sequence of star-forming galaxies*, *ApJ* **660**, L43 (2007) [arXiv:astro-ph/0701924].
- [4] G. Rodighiero, E. Daddi, I. Baronchelli, A. Cimatti et al. *The lesser role of starbursts in star formation at $z = 2$* , *ApJL* **739**, L40 (2011) [arXiv:astro-ph/0701924].
- [5] N. Reddy, M. Pettini, C. Steidel, A. Shapley et al. *The characteristic star formation histories of galaxies at redshifts $z \sim 2 - 7$* , *ApJ* **754**, 25 (2012) [arXiv:1205.0555].
- [6] B. Salmon, C. Papovich, S. Finkelstein, V. Tilviy et al. *The relation between Star Formation Rate and Stellar Mass for Galaxies at $3.5 \leq z \leq 6.5$ in CANDELS*, *ApJ* **799**, 183 (2015) .
- [7] P. Santini, A. Fontana, M. Castellano, M. Crisienzo et al. *The star formation main sequence in the Hubble Space Telescope Frontier Fields*, *ApJ* **847**, 76 (2017) [arXiv:1706.07059].

- [8] K. Abazajian, J. Adelman-McCarthy, M. Agüeros, S. Allam et al. *The seventh data release of the Sloan Digital Sky Survey*, **ApJ** **182**, 543 (2009).
- [9] A. Renzini, Y. Peng, *An objective definition for the main sequence of star-forming galaxies*, **ApJ** **801**, L29 (2008)[arXiv:1502.01027].
- [10] S. Zhu, W. Brandt, F. Zou, B. Luo et al. *Radio AGN selection and characterization in three Deep-Drilling Fields of the Vera C. Rubin Observatory Legacy Survey of Space and Time*, **MNRAS** **522**, 3506 (2023).
- [11] G. Mountrichas, V. Buat, G. Yang, M. Boquien et al. *Comparison of the star formation in X-ray-selected AGN in eFEDS with that of star-forming galaxies*, **A&A** **663**, A130 (2022).
- [12] G. Mountrichas, V. Buat, G. Yang, M. Boquien et al. *Comparison of star formation histories of AGN and non-AGN galaxies*, **A&A** **667**, A145(2022).
- [13] N. Abdurro'uf, K. Accetta, C. Aerts, V. Silva et al. *The Seventeenth Data Release of the Sloan Digital Sky Surveys: Complete Release of MaNGA, MaStar, and APOGEE-2 Data*, **ApJ** **259**, 2 (2022).
- [14] R. Riffel, N. Mallmann, S. Rembold, G. Ilha, et al. *Mapping the stellar population and gas excitation of MaNGA galaxies with megacubes. Results for AGN versus control sample*, **A&A** **524**, 5640(2023).
- [15] P. Popesso, A. Concas, L. Morselli, C. Schreiber et al. *The main sequence of star-forming galaxies – I. The local relation and its bending*, **MNRAS** **483**, 3213 (2019).
- [16] A. Tomczak, R. Quadri, K. Tran, I. Labbé et al. *The SFR–M \star relation and empirical star formation histories from ZFOURGE at $0.5 < z < 4$* , **ApJ** **817**, 118 (2016).
- [17] Y. Peng, S. Lilly, K. Kovač, M. Bolzonella et al. *Mass and Environment as Drivers of Galaxy Evolution in SDSS and zCOSMOS and the Origin of the Schechter Function*, **ApJ** **721**, 193 (2010) [arXiv:1003.4747].
- [18] P. Popesso, L. Morselli, A. Concas, C. Schreiber et al. *The main sequence of star-forming galaxies–II. A non-evolving slope at the high-mass end*, **MNRAS** **490**, 5285 (2019).
- [19] G. Magdis, E. Daddi, M. Béthermin, M. Sargent et al. *The evolving interstellar medium of star-forming galaxies since $z = 2$ as probed by their infrared spectral energy distributions*, **ApJ** **760**, 6 (2012) [arXiv:1210.1035].
- [20] K. Whitaker, P. Dokkum, G. Brammer, M. Franx *The star formation mass sequence out to $z = 2.5$* , **ApJL** **754**, L29 (2015) [arXiv:1205.0547].
- [21] K. Whitaker, M. Franx, J. Leja, P. Dokkum et al. *Constraining the Low-mass Slope of the Star Formation Sequence at $0.5 < z < 2.5$* , **ApJ** **795**, 104 (2008)[arXiv:1407.1843].
- [22] J. Leja, Joshua S. Speagle, Y. Ting, Benjamin, D. Johnson et al. *A New Census of the $0.2 < z < 3.0$ Universe. II. The Star-forming Sequence*, **ApJ** **936**, 165 (2022).
- [23] J. E Thorne, A. Robotham, L. Davies, S. Bellstedt, et al. *Deep Extragalactic Visible Legacy Survey (DEVILS): SED fitting in the D10-COSMOS field and the evolution of the stellar mass function and SFR–M \star relation*, **MNRAS** **505**, 540 (2021).
- [24] S. Leslie, E. Schinnerer, D. Liu, B. Magnelli et al. *The VLA-COSMOS 3 GHz Large Project: Evolution of Specific Star Formation Rates out to $z \sim 5$* , **ApJ** **899**, 58 (2020).
- [25] D. Elbaz, E. Daddi, D. Borgne, M. Dickinson et al. *The reversal of the star formation-density relation in the distant universe*, **A&A** **468**, 33 (2007) [arXiv:astro-ph/0703653].
- [26] L. Boogaard, J. Brinchmann, N. Bouché, M. Paalvastet et al. *The MUSE Hubble Ultra Deep Field Survey-XI. Constraining the low-mass end of the stellar mass–star formation rate relation at $z < 1$* , **A&A** **619**, A27 (2018).
- [27] RE. Skelton, KE. Whitaker, IG. Momcheva et al. *3D-HST WFC3-selected photometric catalogs in the five CANDELS/3D-HST fields: photometry, photometric redshifts, and stellar masses*, **ApJ** **214**, 2 (2014).
- [28] N. Cristello, Fan Zou, W. N. Brandt, Chien-Ting J. Chen et al. *Investigating the Star Formation Rates of Active Galactic Nucleus Hosts Relative to the Star-forming Main Sequence*, **ApJ** **962**, 156 (2024).
- [29] Team, Servs *Spitzer Extragalactic Representative Volume Survey Lockman Hole 2-band Catalog*, **NASA IPAC DataSet** (2020).
- [30] S. Leslie, L. Kewley, D. Sanders, N. Lee *Quenching star formation: insights from the local main sequence*, **MNRAS** **455**, L82 (2015) [arXiv:1509.03632].
- [31] T. Shimizu, R. Mushotzky, M. Meléndez, M. Koss et al. *Decreased specific star formation rates in AGN host galaxies*, **MNRAS** **452**, 1841 (2007) [arXiv:1506.07039].
- [32] K. Schawinski, D. Thomas, M. Sarzi, C. Maraston et al. *Observational evidence for AGN feedback in early-type galaxies*, **MNRAS** **382**, 1415 (2007) [arXiv:0709.3015].
- [33] K. Nandra, A. Georgakakis, C. Willmer, M. Cooper et al. *AEGIS: The color-magnitude relation for X-ray-selected active galactic nuclei*, **ApJ** **660**, L11 (2007).
- [34] M. Martig, F. Bournaud, R. Teyssier, A. Dekel et al. *Morphological quenching of star formation: making early-type galaxies red*, **ApJ** **707**, 250 (2009)[arXiv:0905.4669].
- [35] F. Belfiore, R. Maiolino, K. Bundy, K. Masters et al. *SDSS IV MaNGA – sSFR profiles and the slow quenching of discs in green valley galaxies*, **MNRAS** **477**, 3014(2018).
- [36] G. Erfanianfar, P. Popesso, A. Finoguenov, D. Wilman et al. *Non-linearity and environmental dependence of the star-forming galaxies main sequence*, **MNRAS** **455**, 2839 (2016)[arXiv:1511.01899].
- [37] P. Lang, S. Wuyts, R. Somerville, N. Schreiber, R. Genzel et al. *Bulge Growth and Quenching since $z = 2.5$ in CANDELS/3D-HST*, **ApJ** **788**, 788 (2014)[arXiv:1402.0866].
- [38] Bluck, Asa F. L., Maiolino, Roberto, Sánchez, Sebastian F., Ellison, Sara L. et al. *Are galactic star formation and quenching governed by local, global, or environmental phenomena?*, **MNRAS** **492**, 96 (2020).
- [39] D. Croton, V. Springel, S. White, G. Lucia et al. *The many lives of active galactic nuclei: cooling flows, black holes and the luminosities and colours of galaxies*, **MNRAS** **365**, 11 (2013) [arXiv:astro-ph/0508046].
- [40] D. Rosario, P. Santini, D. Lutz, L. Shao et al. *The mean star formation rate of X-ray selected active galaxies and its evolution from $z \sim 2.5$: results from PEP-Herschel*, **A & A** **545**, A45 (2012) [arXiv:1203.6069].

- [41] A. Oemler, L. Abramson, M. Gladders, A. Dressler et al. *The Star Formation Histories of Disk Galaxies: The Live, the Dead, and the Undead*, *ApJ* **844**, 45 (2017).
- [42] E. Tempel, T. Tuvikene, *Merging groups and clusters of galaxies from the SDSS data. The catalogue of groups and potentially merging systems*, *A & A* **602**, A100 (2017) [arXiv:1704.04477]
- [43] P. Ade, N. Aghanim, *Planck 2015 results. XXIII. The thermal Sunyaev-Zeldovich effect—cosmic infrared background correlation*, *A & A* **594**, A23 (2016) [arXiv:1509.06555].
- [44] D. Eisenstein, D. Weinberg, *SDSS-III: Massive spectroscopic surveys of the distant universe, the Milky Way, and extra-solar planetary systems*, *AJ* **142**, 72 (2011) [arXiv:1101.1529].
- [45] S. Alam, F. Albareti, C. Prieto, *The Eleventh and Twelfth Data Releases of the Sloan Digital Sky Survey: Final Data from SDSS-III*, *ApJ* **219**, 12 (2015) [arXiv:1501.00963].
- [46] David J. Schlegel, Douglas P. Finkbeiner, and Marc Davis. *Maps of dust infrared emission for use in estimation of reddening and cosmic microwave background radiation foregrounds*, *ApJ* **500**, 525 (1998).
- [47] Michael A. Strauss, David H. Weinberg, Robert H. Lupton, Vijay K. Narayanan et al. *Spectroscopic target selection in the Sloan Digital Sky Survey: the main galaxy sample*, *AJ* **124**, 3 (2002).
- [48] M. Blanton, S. Roweis, *K-corrections and filter transformations in the ultraviolet, optical, and near-infrared*, *Astronomical Journal* **133**, 734 (2007) [arXiv:astro-ph/0606170].
- [49] M. Blanton, D. Hogg, N. Bahcall, J. Brinkmann et al *The galaxy luminosity function and luminosity density at redshift $z = 0.1$* , *AJ* **592**, 819 (2003) [arXiv:astro-ph/0210215].
- [50] E. Tempel, E. Tago, L. Liivamägi *Groups and clusters of galaxies in the SDSS DR8-Value-added catalogues*, *A & A* **540**, A106 (2012) [arXiv:1112.4648].
- [51] E. Tempel, A. Tamm, M. Gramann, *Flux- and volume-limited groups/clusters for the SDSS galaxies: catalogues and mass estimation*, *A & A* **566**, A1 (2014) [arXiv:1402.1350].
- [52] N. M. Ball, J. Loveday, R. J. Brunner, I. K. Baldry, J. Brinkmann et al. *Bivariate galaxy luminosity functions in the Sloan Digital Sky Survey*, *MNRAS* **373**, 845 (2006).
- [53] P Schechter. *An analytic expression for the luminosity function for galaxies.*, *ApJ* **203**, 297 (1976).
- [54] X. Deng, Y. Xin, P. Wu, P. Jiang et al. *Some Properties of Active Galactic Nuclei in the Volume-limited Main Galaxy Samples of SDSS DR8*, *ApJ* **754**, 82 (2012).
- [55] G. Kauffmann, S. White, *The Environmental Dependence of the Relations between Stellar Mass, Structure, Star Formation and Nuclear Activity in Galaxies*, *MNRAS* **353**, 713 (2004) [arXiv:astro-ph/0402030].
- [56] J. Brinchmann, S. Charlot, *The physical properties of star forming galaxies in the low redshift universe*, *MNRAS* **351**, 1151 (2004) [arXiv:astro-ph/0311060].
- [57] C. Tremonti, T. Heckman, *The Origin of the Mass–Metallicity Relation: Insights from 53,000 Star-Forming Galaxies in the SDSS*, *ApJ* **613**, 898 (2004) [arXiv:astro-ph/0405537].
- [58] C. Kennicutt, *Star Formation in Galaxies Along the Hubble Sequence*, *A&A* **39**, 189 (1998) [arXiv:astro-ph/9807187].
- [59] S. Salim, J. Lee, R. Davé, *On the Mass-Metallicity-Star Formation Rate Relation for Galaxies at $z \sim 2$* , *ApJ* **808**, 14pp (2015) [arXiv:1506.03080].
- [60] S.F. Sanchez, V. Avila-Reese, H. Hernandez-Toledo, E. Cortes-Suarez et al. *SSDSS IV MaNGA - Properties of AGN host galaxies*, *Revista mexicana de astronomía y astrofísica* **54**, 1 (2018).
- [61] R. Cid Fernandes, G. Stasinska, A. Mateus and N. Vale Asari *A comprehensive classification of galaxies in the Sloan Digital Sky Survey: how to tell true from fake AGN*, *MNRAS* **413**, 1687 (2011).
- [62] L. Kewley, B. Groves, G. Kauffmann, T. Heckman et al. *The host galaxies and classification of active galactic nuclei*, *MNRAS* **372**, 961 (2006) [arXiv:astro-ph/0605681].
- [63] G. Kauffmann, T. Heckman, C. Tremonti, J. Brinchmann et al. *The host galaxies of active galactic nuclei*, *MNRAS* **346**, 1055 (2003) [arXiv:astro-ph/0304239].
- [64] L. Kewley, M. Dopita, R. Sutherland, C. Heisler et al. *Theoretical modeling of starburst galaxies*, *ApJ* **556**, 121 (2001) [arXiv:astro-ph/0106324].
- [65] R. Singh, G. van de Ven, K. Jahnke, M. Lyubenova et al. *The nature of LINER galaxies*, *A&A* **558**, A43 (2013)
- [66] Sebastián F. Sánchez *Spatially Resolved Spectroscopic Properties of Low-Redshift Star-Forming Galaxies*, *ARA&A* **99**, 58 (2020).
- [67] Sánchez, S. F., Walcher, C. J., Lopez-Cobá, C. Barrera-Ballesteros, J. K. *From Global to Spatially Resolved in Low-Redshift Galaxies*, *Revista Mexicana de Astronomía y Astrofísica* **57**, 3 (2021).
- [68] E. Daddi, M. Dickinson, G. Morrison, R. Chary et al. *Multiwavelength study of massive galaxies at $z \sim 2$. I. Star formation and galaxy growth*, *ApJ* **670**, 156 (2007). [arXiv:0705.2831].
- [69] J. Rich, L. Kewley, M. Dopita, *Galaxy-Wide Shocks in Late-Merger Stage Luminous Infrared Galaxies*, *ApJ* **782**, 9 (2014) [arXiv:1104.1177].
- [70] T. Yuan, L. Kewley, D. Sanders, *The Role of Starburst-Active Galactic Nucleus Composites in Luminous Infrared Galaxy Mergers: Insights from the New Optical Classification Scheme*, *ApJ* **709**, 884 (2010)
- [71] T. Gonçalves, D. Martin, K. Menéndez-Delmestre, T. Wyder et al. *Quenching star formation at intermediate redshifts: downsizing of the mass flux density in the green valley*, *ApJ* **759**, 67 (2012) [arXiv:1209.4084].
- [72] J. Moustakas, A. Coil, J. Aird, M. Blanton, R. Cool et al. *Quenching star formation at intermediate redshifts: downsizing of the mass flux density in the green valley*, *ApJ* **767**, 50 (2013) [arXiv:1301.1688].
- [73] S. Faber, C. Willmer, C. Wolf, D. Koo, B. Weiner, J. Newman et al. *Galaxy Luminosity Functions to $z \sim 1$: DEEP2 vs. COMBO-17 and Implications for Red Galaxy Formation*, *ApJ* **665**, 265 (2007) [arXiv:astro-ph/0506044].
- [74] R. Hickox, J. Mullaney, D. Alexander, C. Chen, F. Civanoet al. *Black hole variability and the star formation–active galactic nucleus connection: do all star-forming galaxies host an active galactic nucleus*, *ApJ* **782**, 9 (2014) [arXiv:1306.3218].

- [75] K. Schawinski, C. Urry, B. Simmons, L. Fortson, S. Kaviraj et al. *The green valley is a red herring: Galaxy Zoo reveals two evolutionary pathways towards quenching of star formation in early- and late-type galaxies*, *MNRAS* **440**, 889 (2014).
- [76] X. Deng, P. Wu, X. Qian, C. Luo, *Environmental Dependence of Stellar Mass, Star Formation Rate, Specific Star Formation Rate, and AGN Activity for an Apparent Magnitude Limited Main Galaxy Sample of the SDSS DR7*, *PASJ* **64**, 93 (2012).
- [77] I. Lewis, M. Balogh, R. Propris, W. Couch, R. Bower et al. *The 2dF Galaxy Redshift Survey: the environmental dependence of galaxy star formation rates near clusters*, *MNRAS* **334**, 673 (2002) [arXiv:astro-ph/0203336].
- [78] P. Gomez, R. Nichol, *Galaxy Star-Formation as a Function of Environment in the Early Data Release of the Sloan Digital Sky Survey*, *A&A* **584**, 210 (2003) [arXiv:astro-ph/0210193].
- [79] M. Tanaka, T. Goto, *The Environmental Dependence of Galaxy Properties in the Local Universe: Dependence on Luminosity, Local Density, and System Richness*, *AJ* **128**, 2677 (2004) [arXiv:astro-ph/0411132].
- [80] M. Cooper, J. Newman, *The DEEP2 Galaxy Redshift Survey: The Role of Galaxy Environment in the Cosmic Star-Formation History*, *MNRAS* **383**, 1058 (2008) [arXiv:0706.4089].
- [81] S. Patel, B. Holden, *The Dependence of Star Formation Rates on Stellar Mass and Environment at $z \sim 0.8$* , *ApJ* **705**, L67 (2007) [arXiv:0910.0837].
- [82] G. Mountrichas, G. Yang, V. Buat, B. Darvish et al. *The relation of cosmic environment and morphology with the star formation and stellar populations of AGN and non-AGN galaxies*, *A&A* **675**, A137 (2023).
- [83] G. Mountrichas, G. Yang, V. Buat, B. Darvish et al. *Probing star formation rates and histories in AGN and non-AGN galaxies across diverse cosmic environments and X-ray luminosity ranges*, *A&A* **686**, A229 (2024).
- [84] E. Lacerda, Sebastián F. Sánchez, R. Cid Fernandes, C. López-Cobá et al. *Galaxies hosting an active galactic nucleus: a view from the CALIFA survey*, *MNRAS* **492**, 3073 (2020).
- [85] S. F. Sánchez, R. García-Benito, S. Zibetti, C. J. Walcher et al. *CALIFA, the Calar Alto Legacy Integral Field Area survey*, *A&A* **A36**, 21 (2020).